Available online at www.sciencedirect.com
ScienceDirect
International Journal of Heat and Mass Transfer 51 (2008) 1562–1572
International Journal of HEAT and MASS TRANSFER
www.elsevier.com/locate/ijhmt

Convective heat transfer on a rotating disk with a centred impinging round jet

T. Astarita *, G. Cardone

University of Naples Federico II, DETEC, P.le Tecchio, 80, 80125 Naples, Italy

Received 2 May 2007
Available online 20 September 2007

Abstract

Flow visualisations and heat transfer measurements on a rotating disk, with a relatively small centred jet perpendicularly impinging on it, are accomplished by means of infrared (IR) thermography associated with the heated-thin-foil thermal sensor. Flow visualisations show a strong interaction between the turbulent jet and the laminar boundary layer over the rotating disk. A new governing similitude parameter is introduced and a heat transfer correlation for the Nusselt number at the disk centre is proposed. In most cases, the Nusselt number radial profiles tend to overlap if they are normalised with the Nusselt number computed by means of this correlation.

Keywords: Rotating disk; Jet impingement; Local convective heat transfer; Infrared thermography

1. Introduction

The characteristics of the flow field and of the convective heat transfer distribution in rotating systems are both experimentally and theoretically relevant. Of all the possible geometrical shapes, probably the rotating disk is one of the simplest and many design configurations may be realistically represented by it. As a matter of fact, flywheels, disks turbine blades are attached to, disk brakes and even modern high speed CD-ROMs are all examples of practical applications of this model. Very often, the fluid resistance induced by rotation is irrelevant but there are a number of cases where the disk thermal behaviour is of utmost importance.

A possible way to increase both the local and the average heat transfer rates over a rotating disk is to make use of jets impinging on it. The overall increase of the convective heat transfer coefficient h may be caused by two effects: the increased momentum over the disk connected with the jet flow rate and a possible anticipation of transition to turbulence. For centred jets and relatively small nozzle exit diameters, the former effect enhances the convective heat transfer coefficient mostly near the disk centre, while the latter has an influence further away.

Due to their wide use in many processes, round jets perpendicularly impinging on a stationary surface have been widely investigated; two extensive reviews of these studies are given by Martin [1] and Viskanta [2]. For relatively high values of the ratio between the nozzle-to-surface distance and the nozzle exit diameter, the radial distribution of the convective heat transfer coefficient has a bell shaped profile with a maximum at the stagnation impinging point and a monotonic decrease when radially moving downstream (i.e., outward). At smaller distances and for relatively high Reynolds number values, by starting from the stagnation point the radial h profile practically shows a plateau which extends for nearly half a nozzle diameter D followed by a minimum at about 1.2 D, a second maximum at about 2 D and finally a monotonic decrease [3].

Because of its obvious useful applications, also the distribution of the convective heat transfer coefficient over a disk rotating in still air, in both laminar and turbulent

* Corresponding author. Tel.: +39 081 768 3389; fax: +39 081 239 0364.
E-mail address: astarita@unina.it (T. Astarita).

0017-9310/$ - see front matter © 2007 Elsevier Ltd. All rights reserved.
doi:10.1016/j.ijheatmasstransfer.2007.07.040

Nomenclature

a	constant, dimensionless
b	constant, dimensionless
c	constant, dimensionless
D	nozzle exit diameter, m
h	local convective heat transfer coefficient, W/(m^2 K)
h_0	convective heat transfer coefficient at the disk centre as predicted by Eqs. (16) and (17), W/(m^2 K)
k	thermal conductivity coefficient of air, W/(m K)
Nu	jet Nusselt number ($=hD/k$), dimensionless
Nu_0	jet Nusselt number at $r=0$ ($=h_0D/k$), dimensionless
Nu_r	local Nusselt number ($=hr/k$), dimensionless
Pr	Prandtl number, dimensionless
q_j	Joule heat flux, W/m^2
q_k	conductive tangential heat flux, W/m^2
q_{nc}	heat flux by natural convection to ambient, W/m^2
q_r	radiative heat flux, W/m^2
Q_d	disk induced momentum, N
Q_j	jet momentum rate, N
r	local radius, m
r_t	local radius of transition, m
R	disk radius, m
Re_j	jet Reynolds number ($=VD/v$), dimensionless
Re_R	disk Reynolds number ($=\omega R^2/v$), dimensionless
Re_r	local Reynolds number ($=\omega r^2/v$), dimensionless
Re_{rt}	local Reynolds number of transition ($=\omega r_t^2/v$), dimensionless
T_{aw}	adiabatic wall temperature, K
T_w	wall temperature, K or C
V	initial average jet velocity, m/s
z	nozzle exit to disk distance, m

Greek symbols

δ	boundary layer thickness, m
$\Delta T = T_w - T_{aw}$	Temperature difference, K
ζ	dimensionless nozzle to disk distance ($=z/D$), dimensionless
η	dimensionless nozzle to disk distance ($=z/r$), dimensionless
v	kinematic viscosity coefficient of air, m^2/s
ξ	similitude parameter, dimensionless
ρ^2	square correlation factor
ω	disk angular speed, rad/s

regimes, has been extensively studied in the past; e.g., the papers by Millsaps and Pohlhausen [4] Cobb and Saunders [5], Northrop and Owen [6] and Cardone et al. [7] are herein recalled.

For small values of the local Reynolds number based on the local radius, the induced flow is laminar and the boundary layer thickness turns out to be constant over the disk surface. Consequently, the convective heat transfer coefficient is also independent of the local radius and is practically a sole function of the angular speed:

$$h = ak\sqrt{\frac{\omega}{v}} \tag{1}$$

where h is the above mentioned convective heat transfer coefficient, a is a dimensionless constant, ω the disk angular speed, k and v, respectively, the thermal conductivity and the kinematic viscosity coefficients of air.

The constant of Eq. (1) is a function of the Prandtl number and can be evaluated from the existing exact solution of the governing equations [4]; in particular, for air at ambient temperature ($Pr = 0.71$), a turns out to be equal to 0.33. Often, Eq. (1) is expressed in terms of non dimensional quantities:

$$Nu_r = a\sqrt{Re_r} \tag{2}$$

where Nu_r is the local Nusselt number and Re_r is the local Reynolds number, both based on the local radius r.

For relatively high values of the local Reynolds number, the flow becomes unstable and transition to turbulent flow eventually occurs. Clearly the transitional Reynolds number is strongly dependent on the experimental conditions and generally ranges between 200,000 and 320,000.

In the turbulent regime the convective heat transfer coefficient is an increasing function of the local radius [7] and can be expressed as:

$$Nu_r = 0.0163Re_r^{0.8} \tag{3}$$

The condition of a jet impinging on a rotating surface is more complex because of the interaction between the jet and the boundary layer due to the disk rotation. Several articles analyse the convective heat transfer coefficient from a rotating disk to a uniform stream parallel to the disk axis of rotation such as those of Evans and Greif [8] and Yen et al. [9]. Many other papers report on relatively small non-centred jets: e.g., Metzger et al. [10], Popiel and Boguslawski [11], Brodersen and Metzger [12] and Brodersen et al. [13] and [14]. To the authors' knowledge, only few works consider a small centred jet.

Chen et al. [15] study the local convective heat transfer coefficient over a rotating disk with, and without, an impinging jet by means of the naphthalene sublimation technique. Experiments carried out on the disk with no jet appear to be in agreement with those already existing in the literature. The majority of the authors' work deals with non-centred jets but they also show one test for a cen-

tred jet at a short distance ($z/D = 5$, where z is the nozzle exit to disk distance) and a high jet Reynolds number equal to 60,000. In this case, the Sherwood number appears to be constant on most of the disk surface.

Saniei and Yan [16] perform an experimental study of the local convective heat transfer coefficient over a rotating disk, with and without an impinging jet, by means of a transient liquid crystal technique. Experimental data relative to the rotating disk with no jet shows a maximum of the local Nusselt number at the disk centre also in the laminar regime. Although they ascribe this effect to the development of the boundary layer, present authors believe that this behaviour may be due to some local conduction effects. Some tests are also performed with a rather small ($D/2R = 0.09$, where R is the disk radius) centred jet impinging at a short distance ($z/D \leqslant 6$). Two possible regimes are found, namely jet and disk dominated flows, but neither correlations, nor a significant amount of experimental data, are presented.

The previous discussion shows a lack of both experimental and numerical data on the problem at hand. The purpose of the present work is to perform, by means of IR thermography, some flow visualisations and measurements of the local convective heat transfer coefficient distribution on a rotating disk with a relatively small centred jet perpendicularly impinging on it.

Experiments are performed for testing conditions that assure a laminar boundary layer over almost the whole disk on account of its sole rotation.

The use of IR thermography for such types of problems may be advantageous because of its excellent spatial resolution and thermal sensitivity. Moreover, the use of thermography satisfies both qualitative and quantitative requirements. The main features of this measurement technique are (Carlomagno [17] and Carlomagno and de Luca [18]): it is non-intrusive; it allows a complete two-dimensional mapping of the surface to be tested; digital image processing may be used to treat the infrared camera output.

Cardone et al. [7] already performed detailed measurements of the local convective heat transfer coefficient on a disk rotating in still air by using the same measuring technique; for this reason results relative to the rotating disk with no jet are not going to be presented herein. The experimental apparatus used shows the onset of transition for $Re_r \cong 250{,}000$ [7].

2. Experimental apparatus

A sketch of the experimental apparatus is shown in Fig. 1. The disk section consists of a printed circuit board glued on a 20 mm thick polystyrene foam slab which is contained in a 450 mm diameter ($R = 225$ mm) steel cup. The circuit is used to generate, by Joule effect, a heat flux on the disk external surface exposed to the jet, whereas the foam thermally insulates its inner surface. The printed circuit board is designed to achieve a constant heat flux over the disk; therefore the thickness and width of its conducting tracks, which are located on the disk inner surface, are manufactured with very close tolerances. The tracks, having a double spiral shape, are 35 μm thick, 1.8 mm wide and placed at 2 mm steps; the overall thickness of the board is 0.3 mm. Electric power is supplied to the circuit by means of a Mercotac® rotating electrical connector. In order to enhance the detection of the emitted IR radiation and to reduce the reflected one, the external board surface is coated with a thin layer of black paint which has a total emissivity coefficient equal to 0.95 in the working IR band of the used scanner.

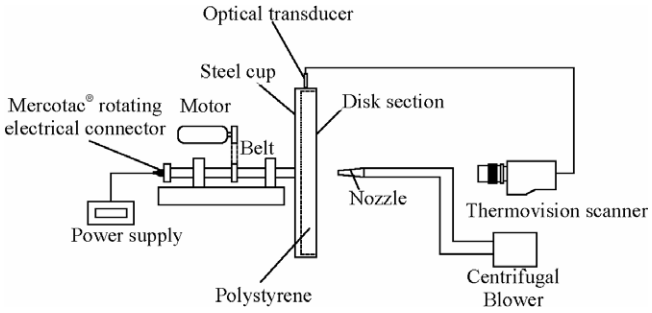

Fig. 1. Experimental apparatus.

A pulley, which is connected by a transmission belt to an electric motor, is fixed on the shaft supporting the disk. By changing the pulley diameter and/or varying the electrical frequency, it is possible to vary the angular speed of the disk in a continuous way within the range 100–4400 rpm.

Air, aspirated by a centrifugal blower, passes through a heat exchanger and a rotameter (both not shown in the Fig. 1) and then goes through a nozzle to generate the jet. The heat exchanger ensures the jet bulk temperature to be practically equal (±0.1 °C) to the temperature of the ambient air the jet mixes with and the rotameter is used to measure the jet initial mass flow rate. Three nozzles with exit diameters equal to 4, 6 and 8 mm, giving a ratio $D/2R$ that varies between 0.0089 and 0.018, are alternatively employed during the tests. The nozzles internal shape is conical and the nozzle exit to disk distance varies between 3 and 75 nozzle exit diameters. The jet always impinges perpendicularly at the centre of the disk surface. The orientation and the position of the nozzle with respect to the disk can be precisely adjusted by means of micrometric screws.

The infrared thermographic scanner used is the AGEMA Thermovision 900. The field of view (which depends on the optics focal length and on the viewing distance) is scanned by the Hg–Cd–Te detector in the 8–12 μm infrared band. Nominal sensitivity, expressed in terms of noise equivalent temperature difference, is 0.07 °C when the scanned object is at ambient temperature. The scanner spatial resolution is 230 instantaneous fields of view per line at 50% slit response function. In order to obtain accurate absolute temperature measurements, the infrared thermographic scanner has been calibrated, by using the procedure reported in [19].

In order to double the effective spatial resolution of the camera, the line scan facility of the IR camera is used to take temperature radial profiles instead of temperature maps of the whole disk. In fact, the thermographic system scans the disk surface along a radius and the complete thermal map of the disk surface is reconstructed by taking into account the disk rotation. By using this technique, it is possible to reconstruct a thermal map that is steady with the disk surface and therefore to visualise the surface temperature distribution over the disk surface. To decrease noise while performing temperature measurements, the thermal profiles acquired by the scanner are averaged in time in order to also accomplish an azimuthal averaging. For each experimental test, about 16,000 lines are used for both map reconstruction and profile average. All the aforesaid manipulations are performed by a dedicated software, which also allows to compute temperature values, heat transfer coefficient and correlations.

An optical transducer, connected to an acquisition board (1 MHz) integrated in the thermographic system, is used to precisely monitor the disk angular speed. For each disk rotation, the optical transducer emits an electrical signal that is recorded by the acquisition board. At the end of each test, an application software is used to calculate both the average and the maximum fluctuations of the angular speed which is always below 1%.

3. Data reduction

The infrared camera measures the temperature map of the disk external surface which is correlated to the heat transfer coefficient by means of the steady state heated-thin-foil technique (Carlomagno and de Luca [18]). In particular, for each pixel of the digitilised thermal image, the local forced convection heat transfer coefficient h is calculated as:

$$h = \frac{q_j - q_r - q_{nc} - q_k}{T_w - T_{aw}} \tag{4}$$

where q_j is the constant Joule heat flux over the disk surface, q_r and q_{nc}, respectively, the net radiative and the natural convection fluxes to ambient, q_k the net conductive flux in the tangential direction (i.e., within the printed circuit board), T_w the wall temperature and T_{aw} the adiabatic wall temperature which, for the present testing conditions, practically coincides with the ambient and jet temperatures.

The radiative thermal losses q_r are computed by means of the measured T_w distribution and of the ambient temperature by using the radiative net flux law (q_r is at worst 25% of the Joule heat flux). Losses due to natural convection and to tangential conduction have been estimated, the first by making "ad hoc" tests and the second by the procedure described in [20]. Both of them resulted negligible with respect to the convective heat flux.

The maximum error in the evaluation of h, Re_R and Re_j, determined by an uncertainty analysis based on the method of Kline and McClintok [21], is mostly found to be less than ±12%, ±2% and ±7%, respectively. It is important to note that, for a given disk heating rate, the highest error occurs where the convective heat transfer coefficient is the largest. In fact, as shown by Eq. (4), for this condition, the temperature difference is the smallest and small absolute errors in temperature evaluation may produce significant errors while computing h.

4. Analysis

A simple application of dimensional analysis allows to determine all the fundamental dimensionless parameters that govern the physical phenomenon herein investigated. In addition to the Prandtl number, which for the present tests is practically constant, it is possible to identify the following five dimensionless groups:

$$Re_R = \frac{\omega R^2}{\nu} \tag{5}$$

$$Re_j = \frac{VD}{\nu} \tag{6}$$

$$Nu = \frac{hD}{k} \tag{7}$$

$$\zeta = z/D \tag{8}$$

$$\eta = z/r \tag{9}$$

where V is the initial average jet velocity.

Re_r is the usual definition of the local Reynolds number for a rotating disk, Re_j is the jet Reynolds number, Nu is the Nusselt number based on the nozzle diameter, while the last two parameters are dimensionless linear scales. Alternatively, as already mentioned in the introduction, it is possible to define a Nusselt number based on the local disk radius:

$$Nu_r = \frac{hr}{k} \tag{10}$$

which is a combination of (7)–(9). While presenting results, another useful parameter is the disk Reynolds number, based on the disk radius and defined as:

$$Re_R = \frac{\omega R^2}{\nu} \tag{11}$$

which in the present test practically represents a dimensionless disk angular speed.

For the conditions herein studied, in order to reduce the number of governing parameters and because of the lack of theoretical analysis, it is necessary to find a reasonable way to evaluate the relative importance of the jet influence with respect to that due to disk rotation. On the assumption that the heat transfer coefficient depends on the flow momentum rate, a possible dimensionless similitude parameter representing the ratio between the two momentum rates (one due to the jet and the other to the rotation of the disk) may be introduced.

The momentum rate of the jet is obviously proportional to:

Table 1
Range of testing parameters

Variable	Minimum	Maximum
ξ	0.1	100
z/D	3	75
Re_j	1400	24,000
Re_R	9000	320,000
D	4 mm	8 mm
V	2.7 m/s	92 m/s
z	24 mm	600 mm
ω	25 rpm	900 rpm
q_j	300 W/m^2	1700 W/m^2

$$Q_j = \rho V D^2 V \tag{12}$$

while, the rate of momentum induced by the rotating disk is proportional to:

$$Q_d = \rho \omega r \cdot r\delta \cdot \omega r \tag{13}$$

where δ is the local boundary layer thickness. Of course, in (13) it is necessary to choose a proper local radius that has to be linked to the physical phenomenon.

Since the present testing conditions foresee relatively high values of z/D, it is well known that, under these circumstances, the jet width is proportional to the distance from the nozzle. The idea is to replace in Eq. (13) the quantity r with the half-width of the jet, which in turn is proportional to z. Furthermore, for a laminar flow over a rotating disk, the boundary layer thickness is constant and proportional to the square root of the ratio between the kinematic viscosity coefficient and the angular speed. Therefore, by recalling the definitions (5) and (6), the governing similitude parameter, proportional to the ratio of the two momentum rates Q_j and Q_d, can be written as:

$$\xi^2 = \frac{Re_j^2}{Re_r^{3/2}\left(\frac{z}{r}\right)^3} = \frac{Re_j^2}{Re_R^{3/2}}\left(\frac{D}{z}\frac{R}{D}\right)^3 = Re_j^2\left(\frac{\nu}{\omega z^2}\right)^{\frac{3}{2}} \tag{14}$$

Of course, in the definition of ξ, various constants, which for sure are not of order one, have been neglected. Therefore, the value of ξ should be always considered as a relative value.

Table 1 shows the ranges of the fundamental parameters used in the present tests. The first four ranges refer to dimensionless quantities while the following four are dimensional variables and, in a way, redundant; q_j values indicate the range of the heat flux rates used during this experimental investigation.

5. Flow visualisations

Experimental results will be presented first in the form of reconstructed temperature maps, then in a quantitative way. As it can be inferred from Eq. (4), by neglecting the radiative heat flux and on account of the constant heat flux boundary condition, the temperature difference is inversely proportional to the convective heat transfer coefficient h; this means that, in the visualisations, higher temperatures correspond to lower heat transfer coefficients and vice versa.

Fig. 2a shows a reconstructed temperature map of the disk rotating at 300 rpm, subjected to a heat flux $q_j = 1170$ W/m^2 and with a centred impinging jet having $Re_j = 11{,}600$. The disk Reynolds number turns out to be $Re_R = 105{,}000$, the similitude parameter ξ is equal to 3.04 and the dimensionless nozzle exit to disk distance is $z/D = 42.5$. The azimuthal averaged temperature difference ΔT profile as a function of the local radius, relative to the same conditions of Fig. 2a, is also shown in Fig. 2b.

The temperature map of Fig. 2a shows an absolute temperature minimum at the disk centre (i.e., a maximum h) and then by moving outward, a monotonic increase. The abrupt decrease of the temperature near the disk limb is clearly due to edge effects. By considering the rotation only, due to the relatively low disk Reynolds number, the flow should be laminar over the whole disk surface. Consequently, the local heat transfer coefficient should be constant and this would result in a constant temperature map [7]. Instead, considering only the jet effect and due to the high z/D value, the temperature distribution should have an absolute minimum at the disk centre (which coincides with the stagnation point) and then increase monotonically when moving outward. The superposition of the two behaviours described above is consistent with what is shown by the reconstructed temperature map of Fig. 2.

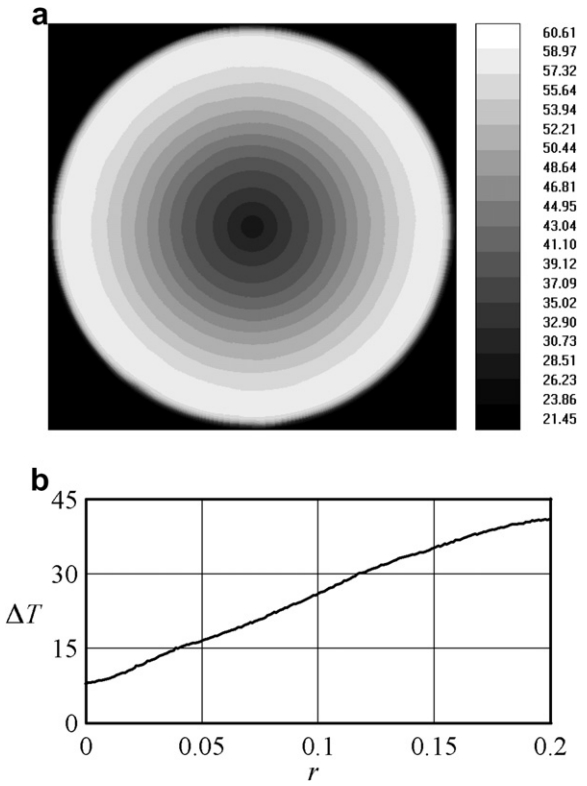

Fig. 2. Temperature map (a) and azimuthal averaged temperature difference profile (b) of the disk at $Re_R = 105{,}000$, $Re_j = 11{,}600$ and $z/D = 42.5$ and $\xi = 3.04$.

By maintaining practically constant both Re_j and ξ while increasing the disk angular speed (500 rpm) the temperature map and ΔT profile of Fig. 3 are obtained (where $q_j = 1130\ \mathrm{W/m^2}$, $z/D = 30.0$, $Re_R = 176{,}000$, $Re_j = 10{,}600$ and $\xi = 3.17$). The reconstructed map appears modified if compared to the previous one because, by moving from the disk centre outward, the temperature initially increases rapidly, reaches an absolute maximum, at about 75% of the disk radius, and then slowly decreases towards the disk limb. As already said to the local maximum in the temperature map correspond a minimum of the local convective heat transfer coefficient.

Also in this case the maximum heat transfer coefficient at the disk centre and its rapid decrease moving outwards are due to the influence of the jet. However, the subsequent increase of h towards the disk limb is not consistent with what expected. Indeed, for $z/D = 30$, the heat transfer coefficient due to the sole jet should monotonically decrease with the local radius. On the other hand, the disk Reynolds number value is, by itself, not sufficient to induce transition from laminar to turbulent flow and, also by considering the sole rotating disk, h should remain constant over the disk [7]. Therefore, the temperature decrease, which occurs towards the disk limb, does not derive from the superposition of the two behaviours and can be only attributed to an interaction of the turbulent jet with the laminar boundary layer over the disk. Indeed, the high turbulence level of the jet tends to shift the transitional instability radius on the disk towards lower values, i.e., inward. Consequently, for increasing local Reynolds number (i.e., increasing radius) values, the induced turbulent boundary layer over the disk tends to be predominant with respect to the jet radial decay resulting in a convective heat transfer coefficient increase towards the disk limb. In that zone, the flow, and consequently the heat transfer, is mainly controlled by the disk rotation so one should refer to it as a *disk dominated regime*.

By practically leaving the values of Re_R and ξ unchanged while almost doubling the jet Reynolds number with respect to the testing conditions of Fig. 3, the temperature map and ΔT profile of Fig. 4 are obtained (where $q_j = 1720\ \mathrm{W/m^2}$, $z/D = 42.5$, $Re_R = 188{,}000$, $Re_j = 20{,}800$ and $\xi = 3.50$). The temperature map shows a monotonically increasing temperature when moving towards the disk limb as in the map reported in Fig. 2. This behaviour may be explained by the higher relative importance of the jet flow with respect to that induced by rotation, i.e., the jet effect prevails over the disk rotation regardless of transition to turbulence, which occurs earlier than in the case of Fig. 3. These flow conditions over the whole disk may be referred as a *jet dominated regime*. Of course, for a much larger disk and identical testing conditions, the temperature

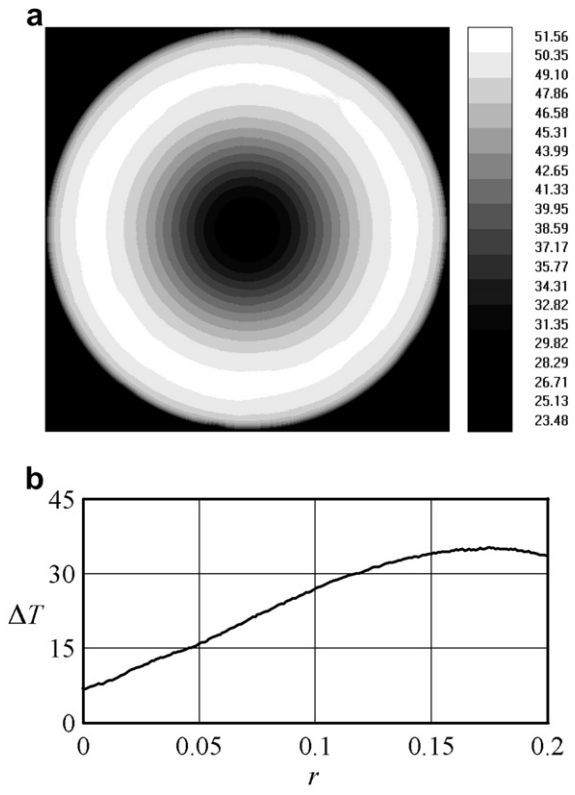

Fig. 3. Temperature map (a) and azimuthal averaged temperature difference profile (b) of the disk at $Re_R = 176{,}000$, $Re_j = 10{,}600$ and $z/D = 30.0$ and $\xi = 3.17$.

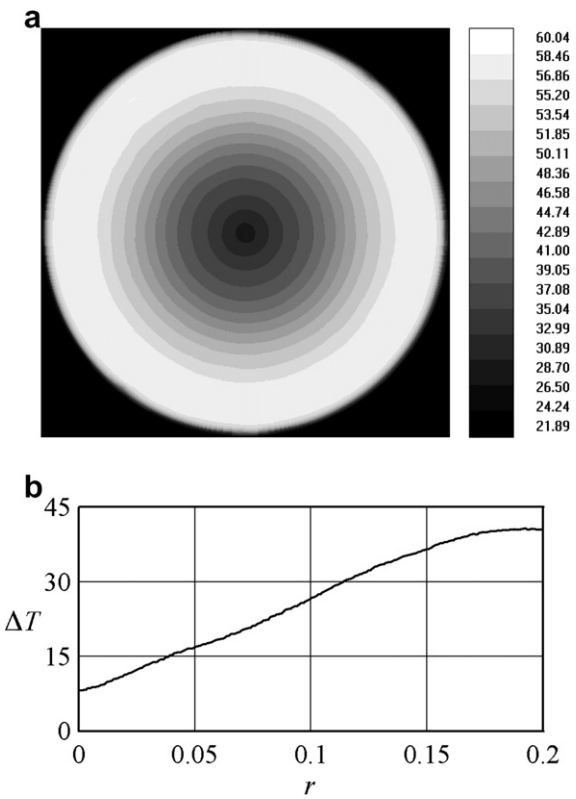

Fig. 4. Temperature map (a) and azimuthal averaged temperature difference profile (b) of the disk at $Re_R = 188{,}000$, $Re_j = 20{,}800$ and $z/D = 42.5$ and $\xi = 3.50$.

(resp., the heat transfer coefficient) should decrease (resp., increase) from a certain radius on because the flow would switch to a disk dominated regime.

6. Quantitative results

First, the convective heat transfer coefficient at the jet flow stagnation point will be examined. By considering only the disk rotation the flow should be always laminar at the disk centre and h can be evaluated from Eq. (1). If the analysis developed in paragraph 4 is correct, with regard to the case of a jet impinging on a rotating disk, the h departure from the latter value should be a function of ξ only. Therefore, it seems reasonable to plot the dimensionless parameter $h_0/k\sqrt{\nu/\omega} = Nu_r/\sqrt{Re_r}$, measured at the disk centre, as a function of the similitude parameter ξ.

A wide set of testing conditions is investigated in order to correlate the data in this way and the experimental results are shown in Fig. 5. Data of this figure refer to more than 160 tests performed by randomly varying within the ranges indicated in Table 1: the disk angular speed, the nozzle diameter, the jet initial flow rate and the nozzle to disk distance. As mentioned before since the similitude parameter should hold only for high values of the z/D ratio, even if randomly chosen, z always fulfils the requirement that $z/D > 14$.

An attempt has been made to correlate all the measured data by an equation having the form:

$$\frac{h_0}{k}\sqrt{\frac{\nu}{\omega}} = 0.33 + b\xi^c \tag{15}$$

where the constants b and c turn out to be, $b = 1.342$ and $c = 0.688$. This correlation is indicated by the broken line of Fig. 5 but seems to deviate from the experimental data

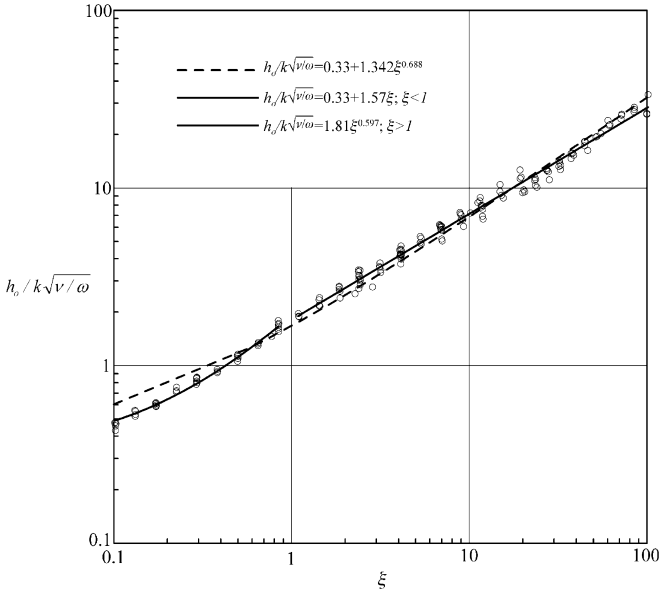

Fig. 5. Normalised convective heat transfer coefficient at the disk centre as a function of the similitude parameter ξ.

especially at low ξ values. In fact, the experimental data shows a different behaviour for small and large values of the similitude parameter. Really, for $\xi > 1$, data appears to be well correlated, in the log–log plane, by a straight line while the same is not true for smaller values of ξ where a linear regression shows a more satisfactory behaviour. Therefore, the equations of the two correlation curves, also shown in Fig. 5 with continuous lines, are:

$$\frac{h_0}{k}\sqrt{\frac{\nu}{\omega}} = 0.33 + 1.57\xi; \quad \text{for } \xi < 1 \quad (\rho^2 = 0.988) \tag{16}$$

$$\frac{h_0}{k}\sqrt{\frac{\nu}{\omega}} = 1.81\xi^{0.597}; \quad \text{for } \xi > 1 \quad (\rho^2 = 0.989) \tag{17}$$

As in Eq. (15), also in Eq. (16) the first constant has been assumed to be equal to 0.33 so that in the limit $\xi \to 0$ (rotating disk without jet) the two equations reduce to Eq. (1) with $a = 0.33$ that, as already mentioned, is the correct value for $Pr = 0.71$. The two above correlations (16) and (17) have been obtained by, respectively, using 42 and 122 data points.

For high ξ values (i.e., predominance of the jet) the convective heat transfer coefficient at the stagnation point can be expressed also in terms of the jet Nusselt number. Indeed, by reformulating Eq. (17) it is obtained:

$$Nu_0 = 1.81\left(\frac{\omega z^2}{\nu}\right)^{0.0523} Re_j^{0.597}\frac{D}{z} \tag{18}$$

The first dimensionless group that appears in Eq. (18) includes the disk angular speed but its exponent turns out to be quite small because the importance of the disk rotation should be weak for $\xi > 1$. The other two exponents are well in accordance with those indicated in the literature for the impinging jet. In particular, for $Re_j > 14{,}600$ and $z/D > 20$, Gardon and Cobonpue [22] report the exponents of the jet Reynolds number and of the D/z ratio to be, respectively, equal to 0.5 and 1.

The dependence of the convective heat transfer coefficient on the radial coordinate will be now analysed starting from the case $\xi < 1$. By using data obtained in the same tests already presented in Fig. 5, the average experimental profile along the dimensionless coordinate r/z of the ratio:

$$\frac{\frac{h}{k}\sqrt{\frac{\nu}{\omega}} - 0.33}{\frac{h_0}{k}\sqrt{\frac{\nu}{\omega}} - 0.33} \tag{19}$$

is reported in Fig. 6 for $z/D > 14$ together with its spread that is estimated by two standard deviations. The local average has been obtained by excluding data involving incidental earlier transition already discussed in Section 5. The denominator of ratio (19) is not a measured value but it is evaluated according to Eq. (16). Naturally, the curve spread of Fig. 6 would be much smaller if the h_0 measured values were used. No further data will be reported for $\xi < 1$.

Results relative to $\xi > 1$ and $z/D > 14$ are shown in Fig. 7 where again the average and the spread of h/h_0 is reported as a function of r/z. Also in this case h_0 is calcu-

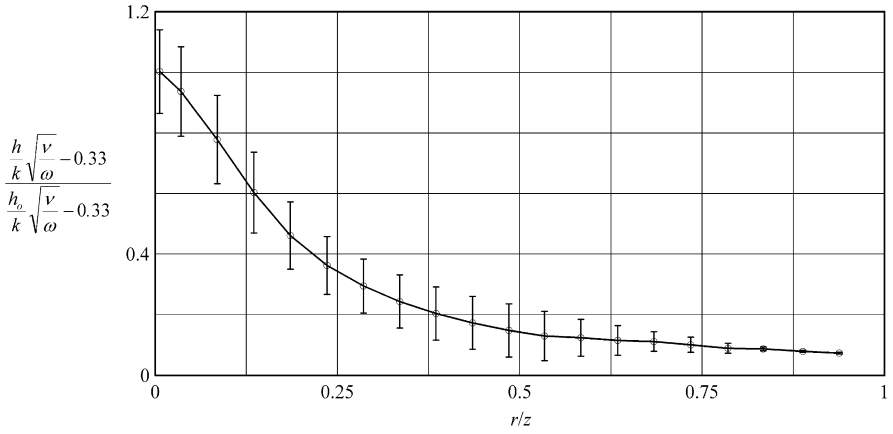

Fig. 6. Averaged normalised convective heat transfer coefficient as a function of r/z for $\xi < 1$ and $z/D > 14$.

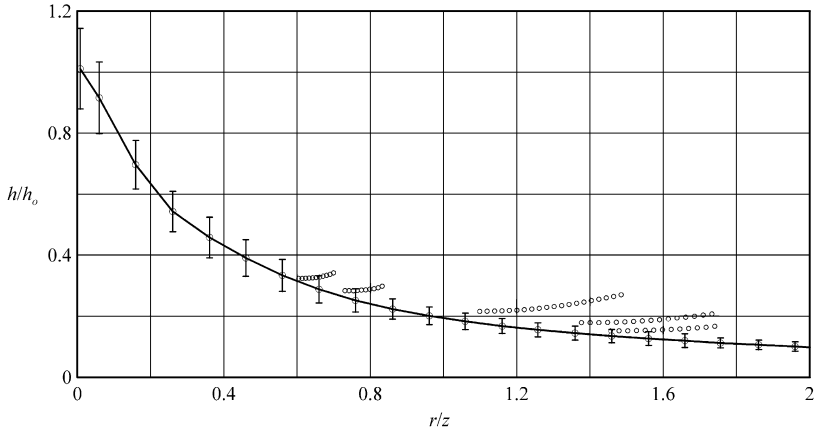

Fig. 7. Averaged normalised convective heat transfer coefficient as a function of r/z for $\xi > 1$ and $z/D > 14$.

lated by means of Eq. (17) and the same 122 different tests presented in Fig. 5 are plotted. For small values of r/z, practically all the experimental profiles collapse on a single curve, and the spread is within the experimental uncertainty. For higher r/z values, as indicated by the five departing curves, a number of tests show a gradual increase of the convective heat transfer coefficient and this, as already said, has to be attributed to the predominance of the induced turbulent boundary layer over the disk with respect to the jet flow, the departing point depending on testing conditions.

Based on the theoretical analysis, ξ should not be a similitude parameter for small values of the z/D ratio, this assertion being supported by data of Fig. 8 at small values

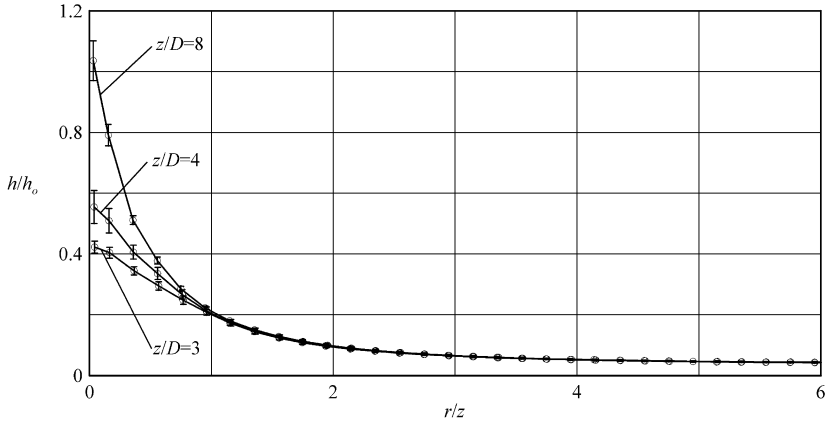

Fig. 8. Averaged normalised convective heat transfer coefficient as a function of r/z for $\xi > 1$ and z/D equal to 3, 4 and 8.

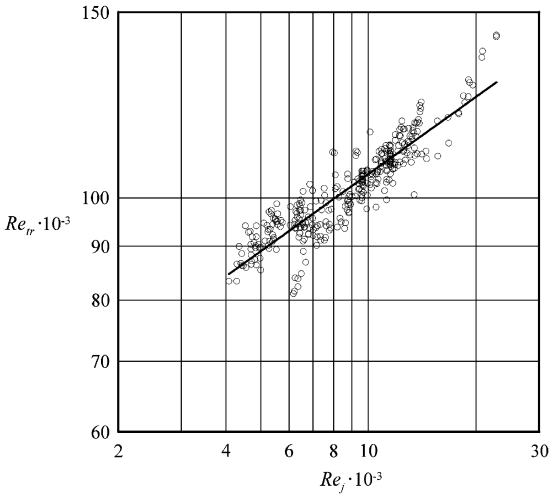

Fig. 9. Transitional Reynolds number as a function of the jet Reynolds number for $\xi > 1$.

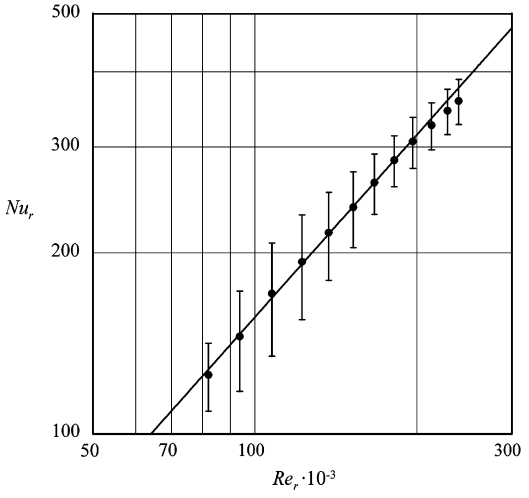

Fig. 10. Averaged local Nusselt number as a function of the local Reynolds number in the disk dominated regime.

of r/z. In this figure, as in the two preceding ones, the average and spread of h/h_0 is plotted as a function of r/z for $\xi > 1$. Data of Fig. 8 are relative to about 70 different testing conditions where z/D is either equal to 3, 4, or to 8. For $r/z > 1$ all the experimental data practically collapse on the same curve and this demonstrates that the introduced similitude parameter holds also for small values of z/D at high r/z values. It is interesting to note that, even if the group of data, for $z/D = 8$ and $r/z = 0$, have not been included in the evaluation of Eq. (17) it is still in good agreement with this prediction.

In order to find a correlation for the transition from jet dominated to disk dominated regime it is necessary to try to clearly define the point of transition from jet to disk dominated regime. An unambiguous way to define the local transition radius r_t is the value of r where the local convective heat transfer coefficient reaches an absolute minimum. By plotting the transitional Reynolds number Re_{rt}, based on r_t, as a function of the jet Reynolds number, the graph of Fig. 9 is obtained where about 340 different points evaluated by randomly varying all the experimental conditions are shown for $\xi > 1$. In this figure, the data spread is quite large due to both the intrinsic difficulties of this type of measurement and to the assumed definition of the local radius of transition. Nevertheless, a power law correlation can be found:

$$Re_{tr} = 11200 Re_j^{0.24} \quad (\rho^2 = 0.830) \tag{20}$$

In the disk dominated regime, Eq. (3) should be recovered and, in order to verify this occurrence, in Fig. 10 the average and spread of Nu_r is plotted as a function of Re_r for $Re_r > Re_t$. Fig. 10 contains results of about 340 different tests and only data (nearly 16,000 measurement points) with $r > r_t$ are considered. Again, the data spread is quite large and, for low Reynolds numbers Re_r, the disk dominated regime is not yet completely established. A power law correlation of the form of Eq. (3) can be found by using a multiplying constant equal to 0.0167 ($\rho^2 = 0.830$). The value of the constant is in good agreement with the experimental data of [7] who obtained 0.0163.

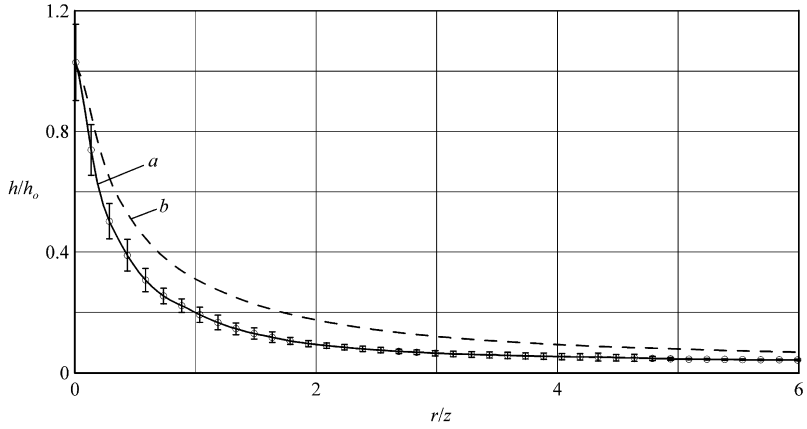

Fig. 11. Normalised convective heat transfer coefficient as a function of r/z for $\xi > 1$: (a) local value and (b) mean value.

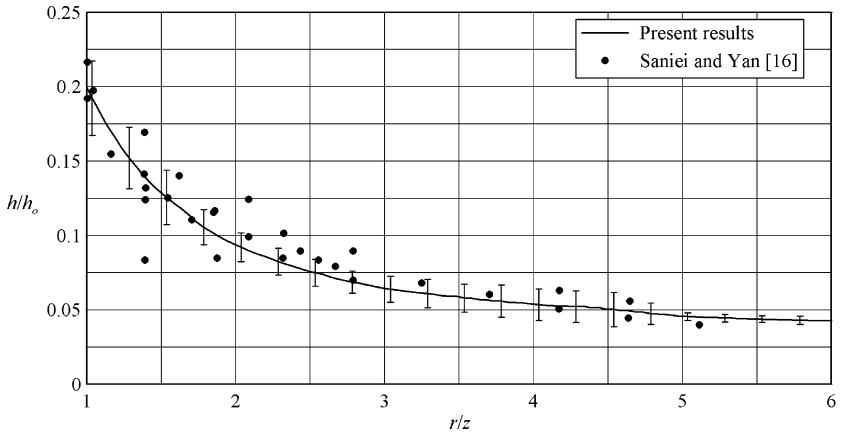

Fig. 12. Normalised convective heat transfer coefficient as a function of r/z for $\xi > 1$: Comparison with data of Saniei and Yan [16].

The sum of all the obtained data is shown in Fig. 11, where the average and spread of h/h_0 is plotted as a function of r/z (solid line); about 750 different tests, relative to $\xi > 1$, summing up more than 130,000 experimental points, are used to construct the figure. In this figure all the experimental test have been cut at the transitional radius according to Eq. (20) and, for this reason, it is not possible to see the gradual increase of the convective heat transfer coefficient due to the transition to disk dominated regime (see Fig. 7). On the other hand, data relative to $z/D < 14$ have been cut for $r/z < 1$ in order to remove the already cited high discrepancies near the impingement point. Fig. 11 shows that the data spread is quite small confirming the validity of ξ as a similitude parameter and of the found correlation of the convective heat transfer coefficient. The normalised convective heat transfer coefficient, averaged over the local enclosed surface (i.e., from 0 up to r/z), is also plotted (dashed line) in Fig. 11 in order to obtain mean measurements. As shown by Fig. 12 a good agreement with the data by Saniei and Yan [16] is found for $r/z > 1$.

7. Conclusions

Local visualisations of the reconstructed thermal maps and quantitative measurements of the convective heat transfer coefficient are performed over a rotating disk with a small centred jet impinging on it. Experimental tests are conducted by varying the nozzle exit diameter, the disk to nozzle distance, the disk angular speed and the initial jet mass flow rate over wide ranges. Infrared thermography and the heated thin-foil steady state technique are used to obtain two-dimensional visualisations and convective heat transfer correlations.

Flow visualisations show a strong interaction between the turbulent jet and the laminar boundary layer over the rotating disk. In particular, for relatively high laminar disk Reynolds numbers and intermediate jet Reynolds numbers, the Nusselt number increase towards the disk limb is a consequence to the interaction of the turbulent jet with the disk boundary layer. Actually, the higher turbulence level of the jet tends to shift the transitional instability on the disk towards lower values of the local Reynolds number, i.e., towards lower local radius.

To correlate the heat transfer tests, it is assumed that the convective heat transfer coefficient depends on the momentum flux. Therefore, a similitude parameter ξ, which is proportional to the ratio between the two momentum fluxes due, respectively, to the jet and to the rotation of the disk, is proposed.

For the present experimental condition two different flow regimes are found for ξ, namely high and low values of the similitude parameter. For small values of ξ and large z/D a correlation for the convective heat transfer coefficient at the disk centre is found; by plotting the quantity of Eq. (19) as a function of r/z, all the profiles seem to overlap within the experimental error as long as no transition to disk dominated flow occurs.

Also for high ξ and z/D values a correlation for the convective heat transfer coefficient at the disk centre is proposed; and again the experimental h profiles normalised by said correlation, if plotted as a function of r/z with no transition to disk dominated flow occurring, collapse on a single curve. For small z/D ratios and near the disk centre, the correlation does not work but, for $r/z > 1$ again the normalised experimental profiles overlap the former curve.

In order to establish the onset of transition to disk dominated flow, a correlation between the rotational Reynolds number of transition and the jet Reynolds number is also proposed.

Acknowledgement

The authors wish to thank Prof. Giovanni Maria Carlomagno for helpful discussion throughout the course of this work.

References

[1] H. Martin, Heat and mass transfer between impinging gas jets and solid surfaces, Adv. Heat Transfer 13 (1977) 1–60.

[2] R. Viskanta, Heat transfer to impinging isothermal gas and flame jets, Exp. Therm. Fluid Sci. 6 (1993) 111–134.
[3] C. Meola, L. de Luca, G.M. Carlomagno, Influence of the shear layer dynamics on impingement heat transfer, Exp. Therm. Fluid Sci. 13 (1996) 29–37.
[4] K. Millsaps, K. Pohlhausen, Heat transfer by laminar flow from a rotating plate, J. Aeronaut. Sci. 19 (1952) 120–126.
[5] E.C. Cobb, O.A. Saunders, Heat transfer from a rotating disk, Proc. Royal Soc. 236 (1956) 343–351.
[6] A. Northrop, J.M. Owen, Heat transfer measurements in rotating-disk systems. Part 1: The free disk, Int. J. Heat Fluid Flow 9 (1) (1988) 19–26.
[7] G. Cardone, T. Astarita, G.M. Carlomagno, Heat transfer measurements on a rotating disk, Int. J. Rotating Machinery 3 (1) (1997) 1–9.
[8] G.H. Evans, R. Greif, Forced flow near a heated rotating disk: A similarity solution, Numer. Heat Transfer 14 (1988) 373–387.
[9] S.C. Yen, J.S. Wang, Mass transfer and fluid flow due to a rotating disk with external forced convection, Therm. Eng. Sci. 17 (8) (1992) 2001–2008.
[10] D.E. Metzger, W.J. Mathis, L.D. Grochowsky, Jet cooling at the rim of a rotating disk, J. Eng. Power 101 (1979) 68–72.
[11] C.O. Popiel, L. Boguslawski, Local heat transfer from a rotating disk in an impinging round jet, J. Heat Transfer 108 (1986) 357–363.
[12] S. Brodersen, D. Metzger, Experimental investigation of the flowfield resulting from the interaction between an impinging jet and a rotating disk, Exp. Therm. Fluid Sci. 5 (1992) 351–358.
[13] S. Brodersen, D.E. Metzger, H.J.S. Fernando, Flows generated by the impingement of a jet on a rotating surface: Part I – basic flow patterns, J. Fluid Eng. 118 (1996) 61–67.
[14] S. Brodersen, D.E. Metzger, H.J.S. Fernando, Flows generated by the impingement of a jet on a rotating surface: Part II – detailed flow structure and analysis, J. Fluid Eng. 118 (1996) 68–73.
[15] Y. Chen, W.T. Lee, S.J. Wu, Heat (mass) transfer between an impinging jet and a rotating disk, Heat Mass Transfer 34 (1998) 195–201.
[16] N. Saniei, X. Yan, An experimental study of heat transfer from a disk rotating in an infinite environment by jet impingement cooling, Enhanced Heat Transfer 7 (2000) 231–245.
[17] G.M. Carlomagno, Thermo-fluid-dynamic application of quantitative infrared thermography, J. Flow Visualization Image Process. 4 (1997) 261–280.
[18] G.M. Carlomagno, L. De Luca, Infrared thermography in heat transfer, in: W.J. Yang (Ed.), Handbook of Flow Visualization, second ed., Taylor & Francis, 2001, pp. 547–573.
[19] T. Astarita, Alcuni Aspetti di Scambio Termico nelle Turbine a Gas, PhD Thesis. University of Naples, 1996.
[20] T. Astarita, G. Cardone, Thermofluidnamic analysis of the flow near a sharp 180° turn channel, Exp. Therm. Fluid Sci. 20 (2000) 188–200.
[21] S.J. Kline, F.A. McClintok, Describing uncertainties in single-sample experiment, Mech. Eng. 75 (1953) 3–8.
[22] R. Gardon, J. Cobonpue, Heat transfer between a flat plate and jets of air impinging on it. In: Proceedings of the Second Heat Transfer Conference, New-York, 1962, pp. 454–460.